Electronic Supplementary Material (ESI) for Journal of Materials Chemistry C.

Supplementary Information

Thermogalvanic Organohydrogel-Based Non-Contact Self-Powered Electronics for Advancing Smart Agriculture

Xinru Yang,[a] Zhiyi Zhang,[b] Saeed Ahmed Khan,[c] Lei Sun,[a] Zhaosu Wang,[a] Xiaojing Cui,[d] Zhiquan Huang*[e] and Hulin Zhang*[a]

[a]College of Electronic Information and Optical Engineering, Taiyuan University of Technology, Taiyuan, 030024, China

[b]College of Materials Science and Engineering, Taiyuan University of Technology, Taiyuan, 030024, China

[c]Department of Electrical Engineering, Sukkur IBA University, Sukkur 65200, Pakistan

[d]School of Physics and Information Engineering, Shanxi Normal University, Taiyuan 030031, China

[e]School of Mechanical Engineering, Taiyuan University of Science and Technology, Taiyuan, 030024, China

*To whom correspondence should be addressed: zhiquanhuang@tyust.edu.cn (Z.H.); zhanghulin@tyut.edu.cn (H.Z.)

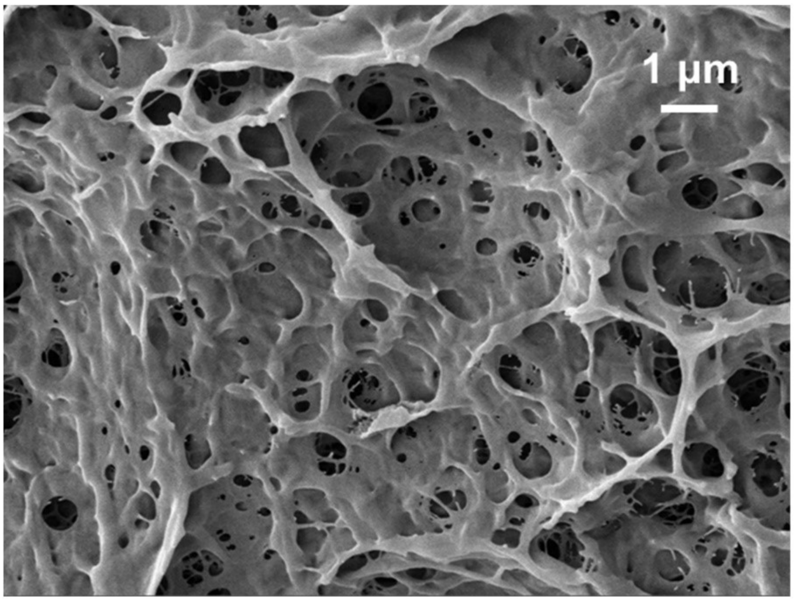

Fig. S1 SEM image of a PVA gel after freeze-drying (scale bar: 1 μm).

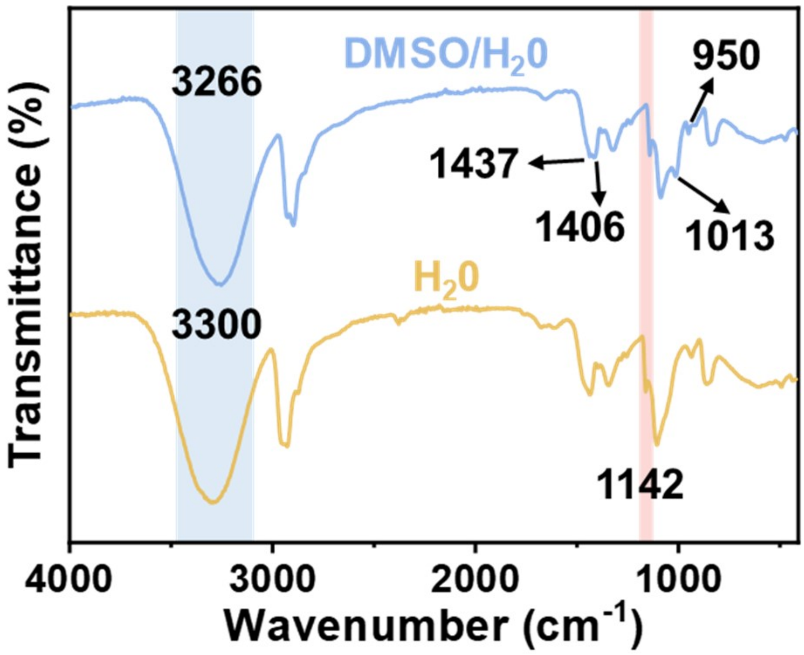

Fig. S2 FTIR spectra of gels with different compositions.

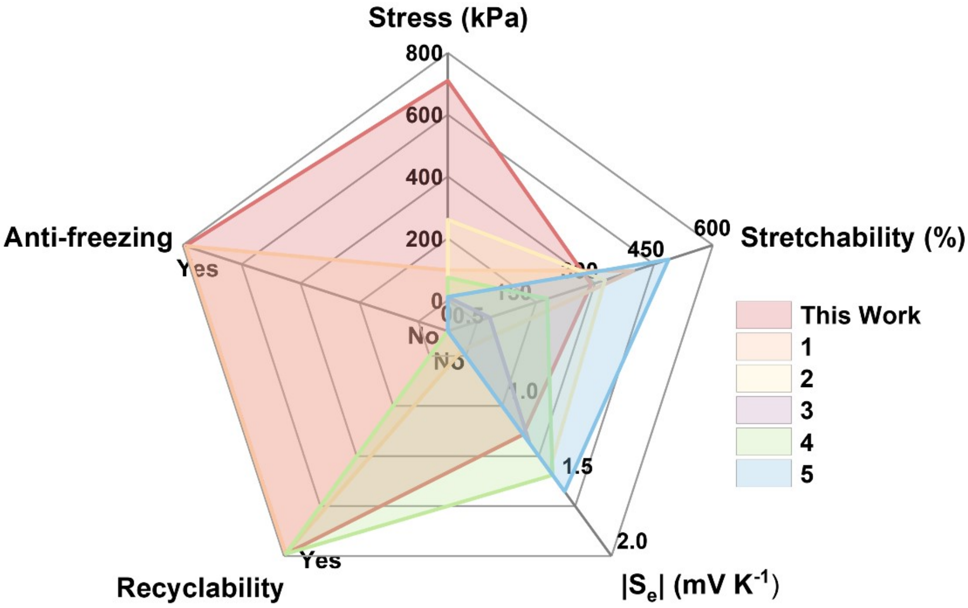

Fig. S3 A comprehensive comparison between the organohydrogel and the previously reported thermogalvanic hydrogels in terms of the comprehensive properties of Stress (kPa), Stretchability (%), Seebeck coefficient (S_e), Recyclability and Anti-freezing.

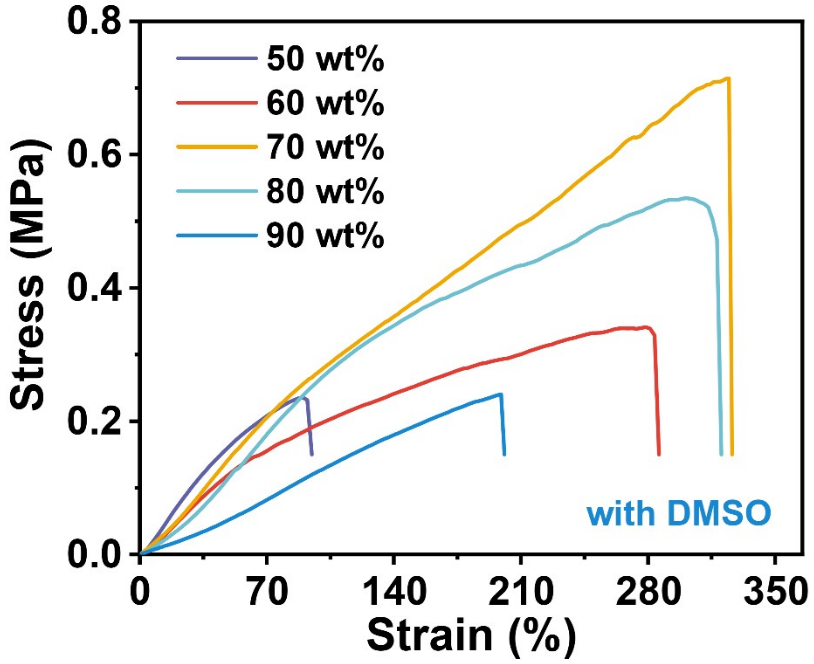

Fig. S4 Stress-Strain curves of the gel with different concentration of the DMSO.

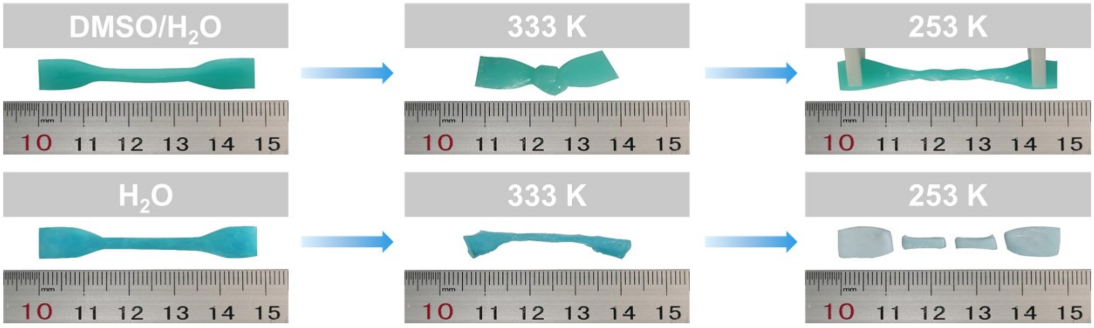

Fig. S5 Elastic stability of the DMSO/H_2O and H_2O hydrogel at 333K and subzero temperatures.

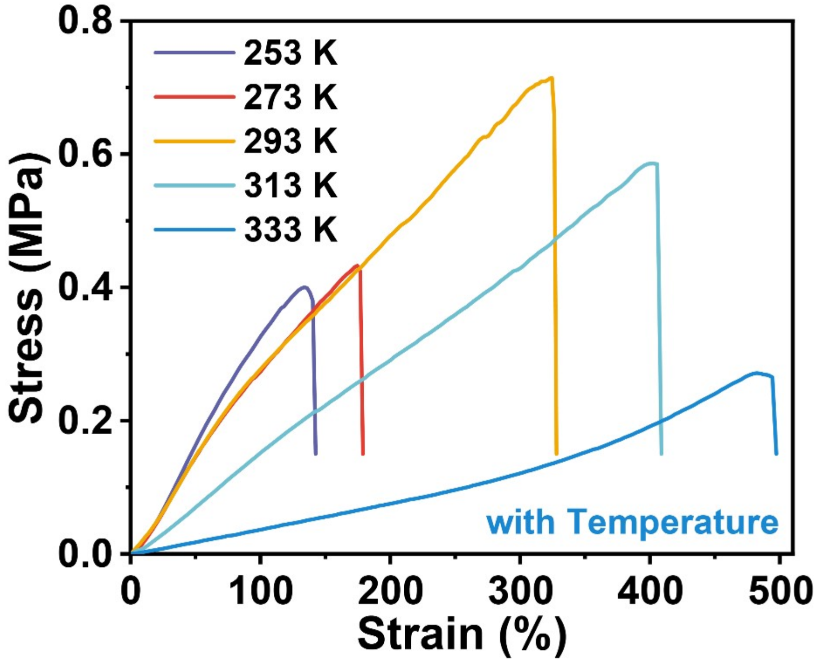

Fig. S6 Stress-Strain curves of the gel under different temperatures.

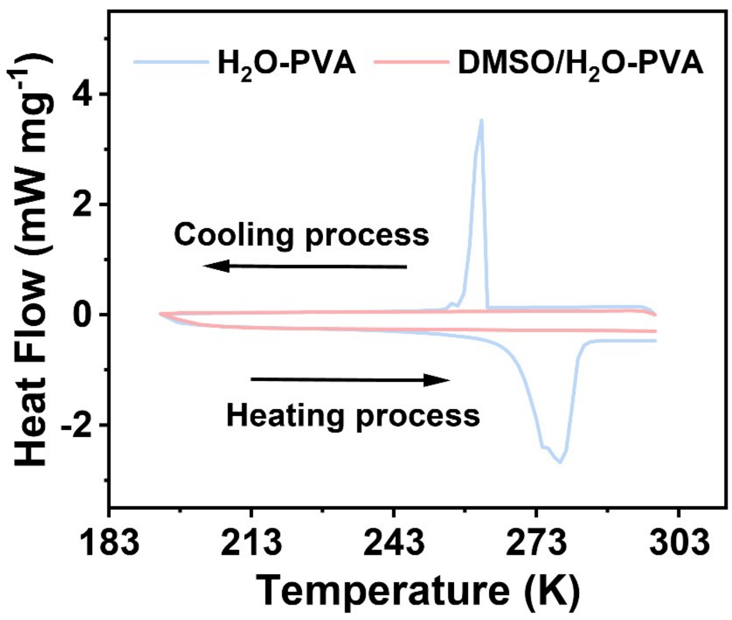

Fig. S7 DSC curves for gels with different compositions.

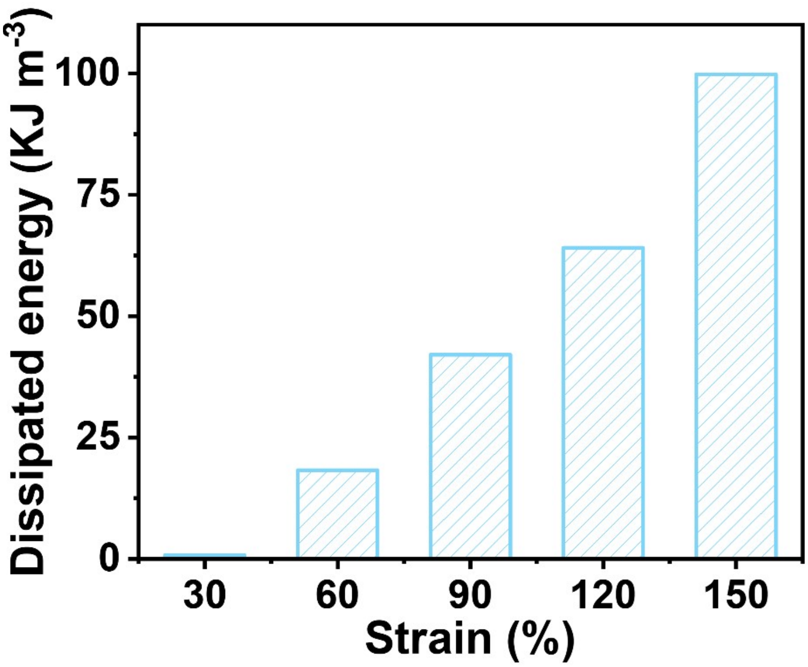

Fig. S8 Dissipated energy values of organohydrogel at different tensile strains.

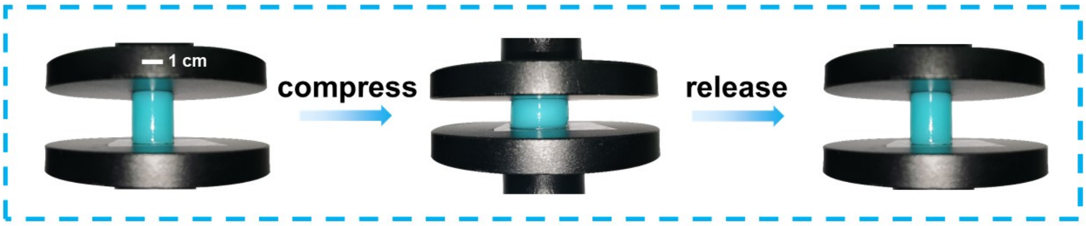

Fig. S9 Photos showing the organohydrogel excellent compressive and recovery.

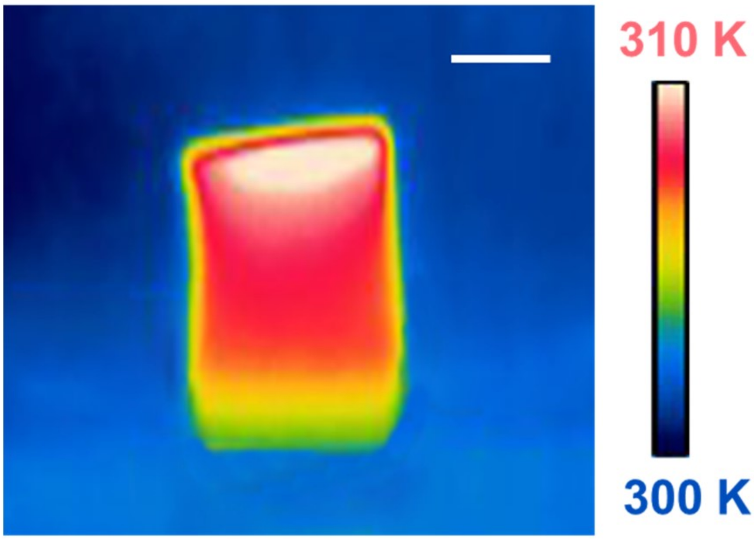

Fig. S10 Infrared image of an organohydrogel exposed to sunlight for 120s (scale bar: 1cm).

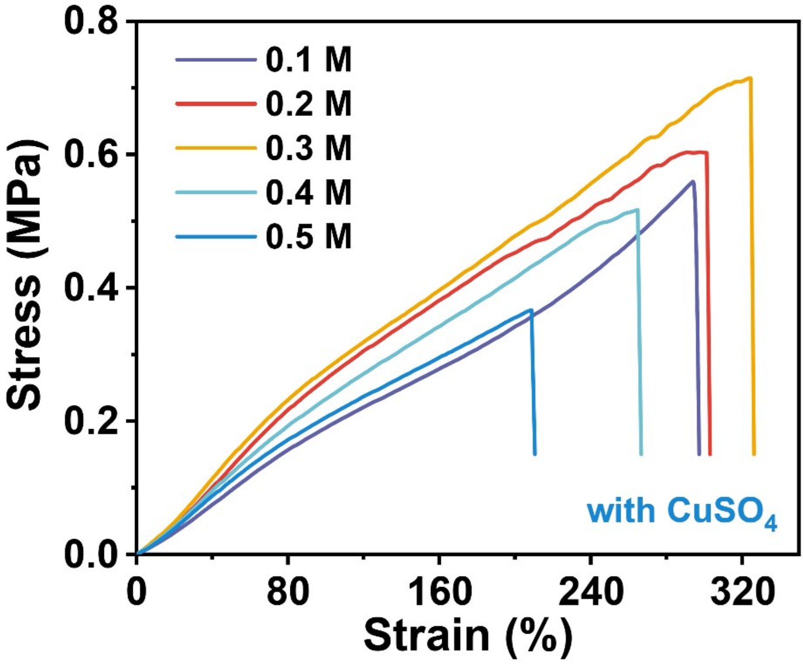

Fig. S11 Stress-Strain curves of the gel with different concentration of the $CuSO_4$.

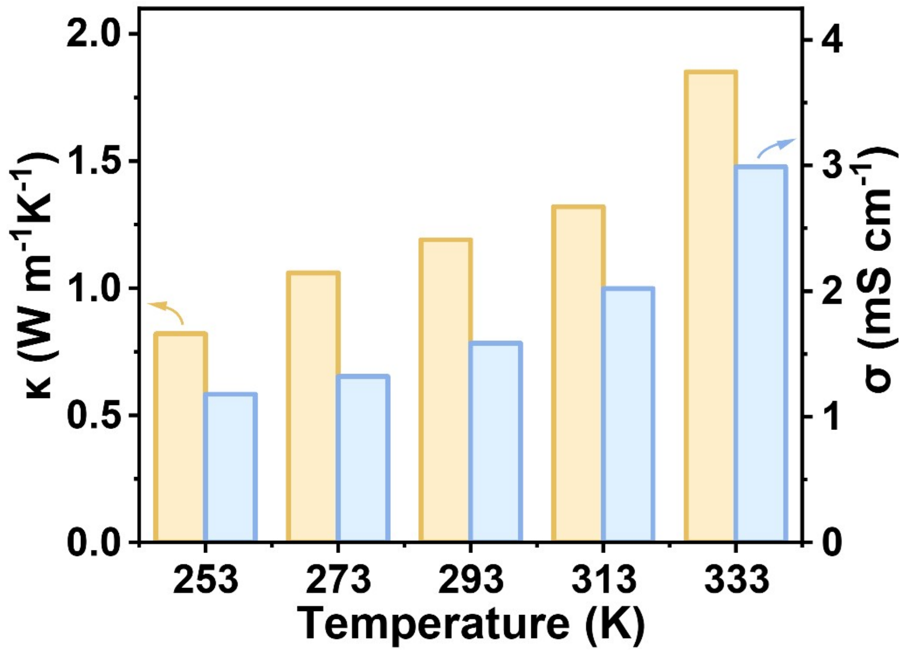

Fig. S12 Electrical and thermal conductivity of organohydrogel at different temperatures.

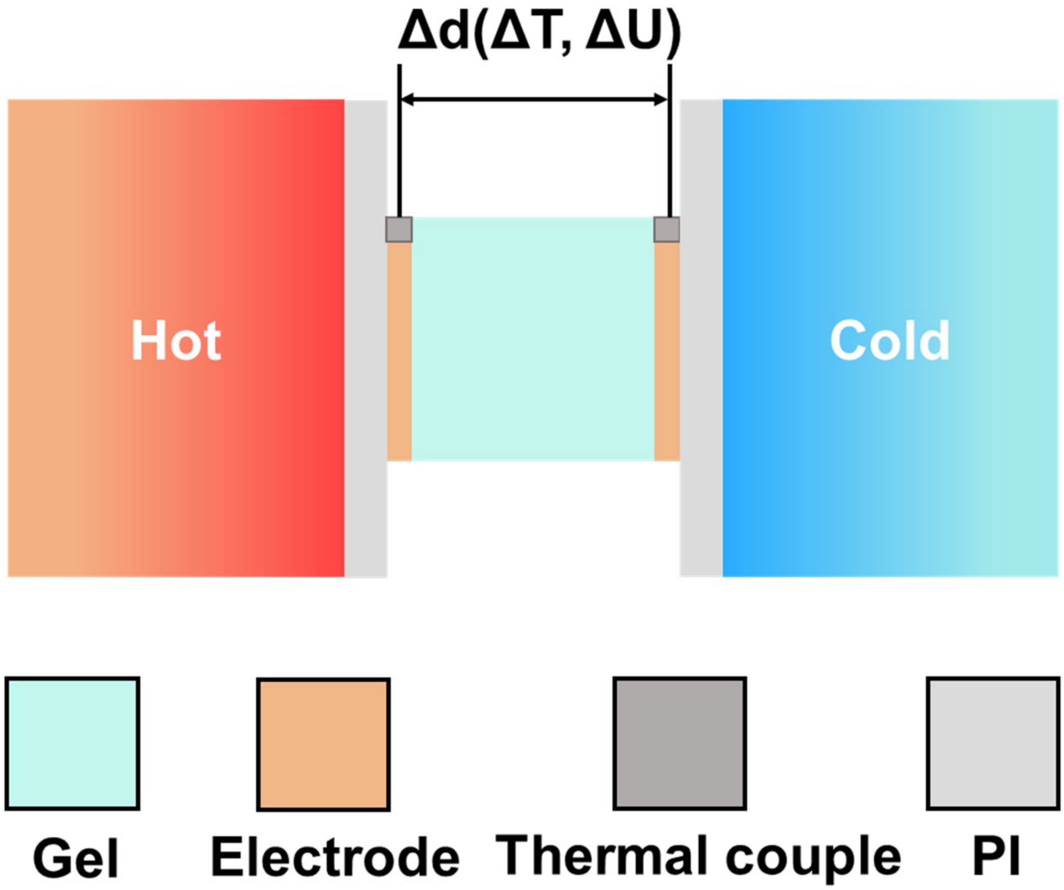

Fig. S13 Schematic image of the platform for thermopower measurements.

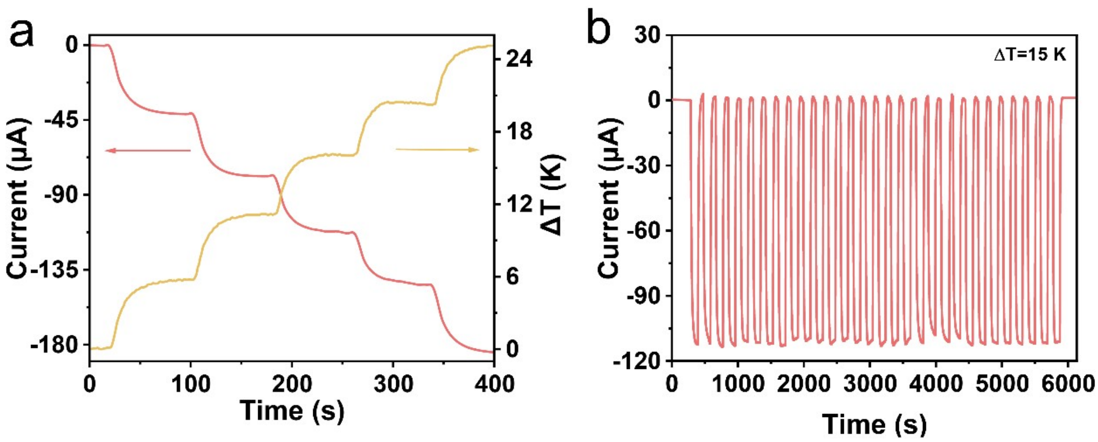

Fig. S14 (a) Thermal current curve of the thermogalvanic gel at different temperatures. (b)Thermal currents in organohydrogel subjected to 30 cycles at ~15 K temperature difference.

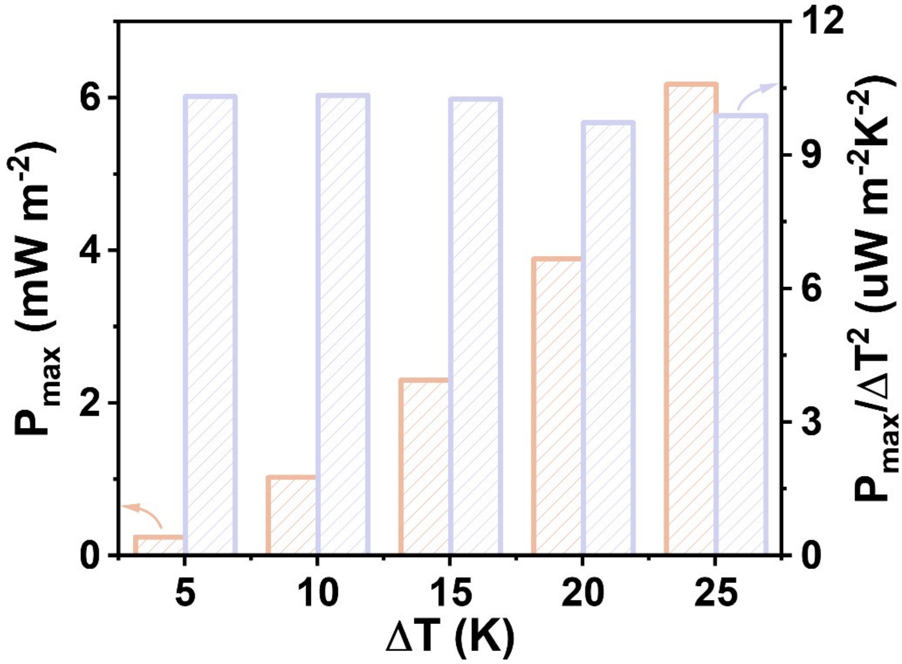

Fig. S15 The maximum output power density and normalized output power density curves under different ΔT values.

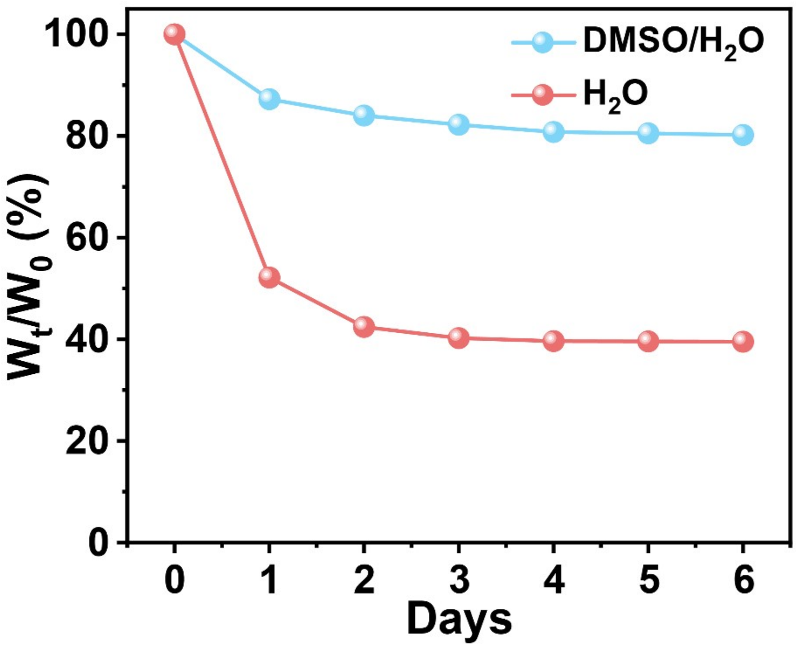

Fig. S16 Comparison of anti-drying capacity of the DMSO/H_2O and H_2O gel over 6 days at room temperature.

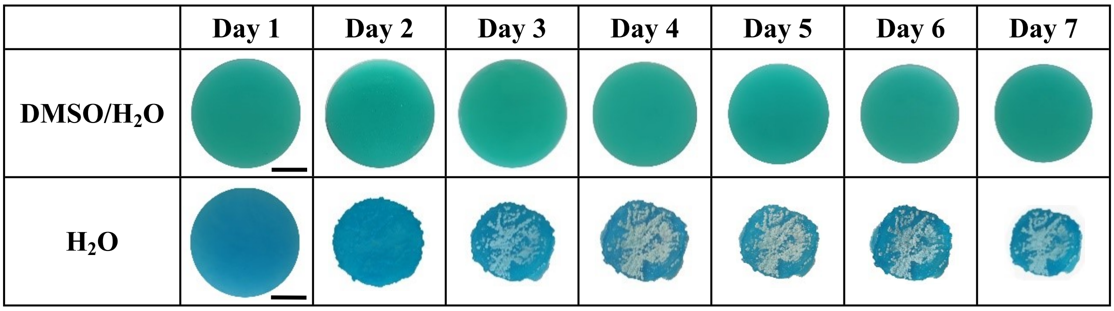

Fig. S17 Images of the DMSO/H_2O and H_2O gel at different different intervals (Scale bar: 1 cm).

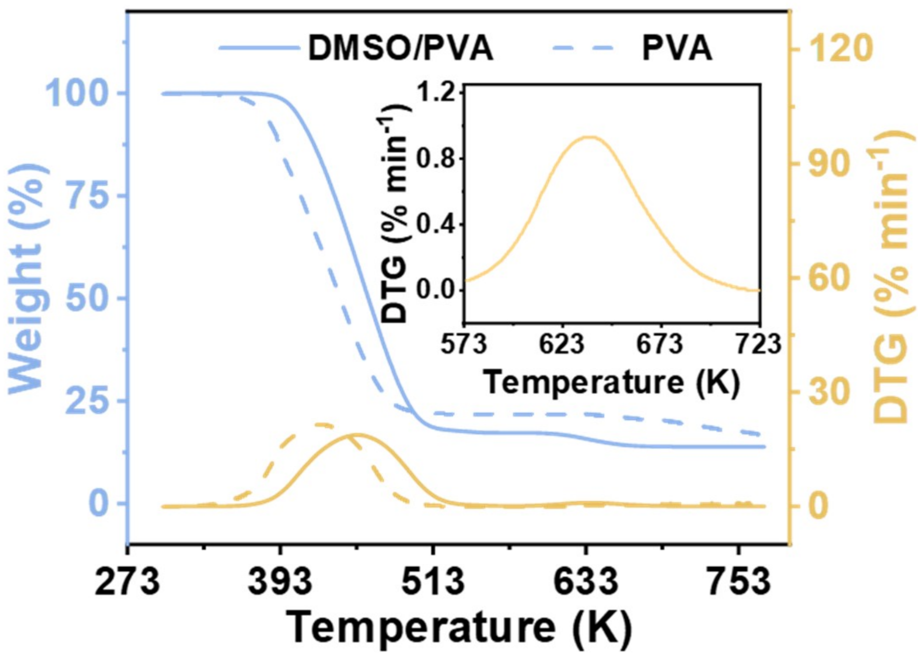

Fig. S18 TG and DTG curves of gels with or without DMSO.

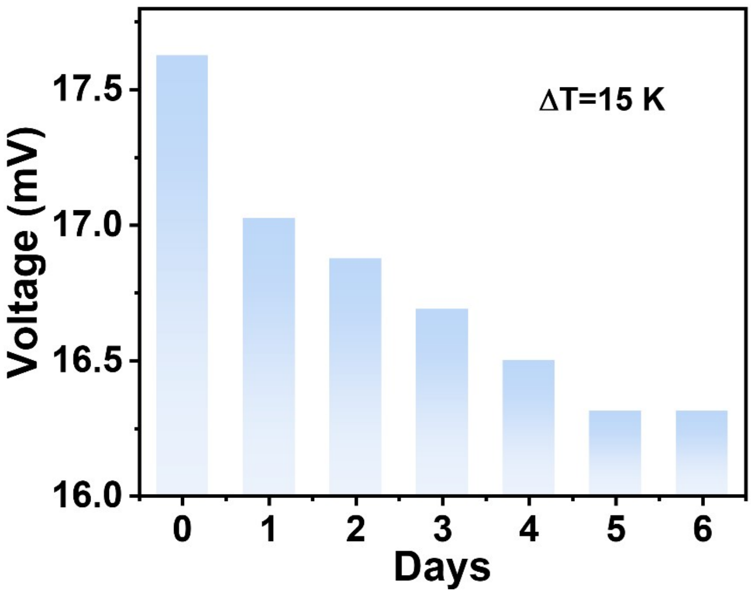

Fig. S19 Variation of open circuit voltage after being placed in the air for 6 days.

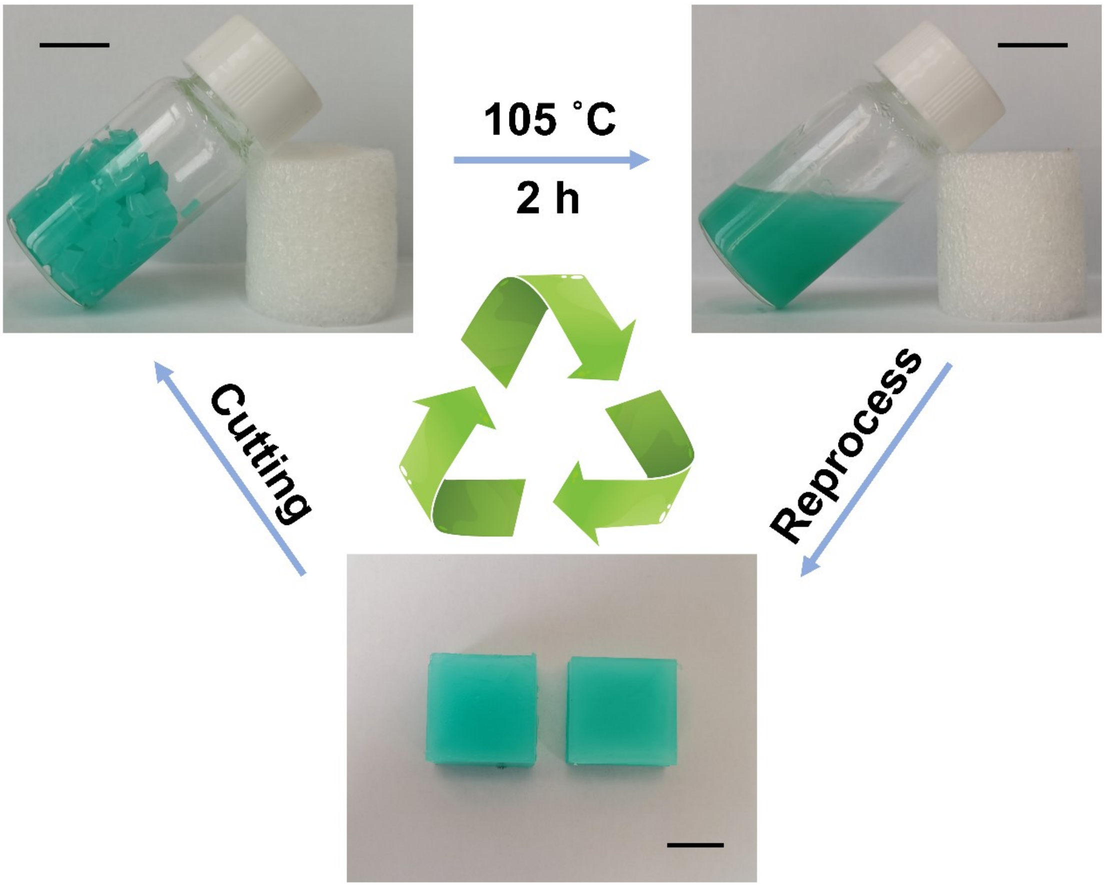

Fig. S20 Recycling process of the organohydrogel. Scale bar 1 cm.

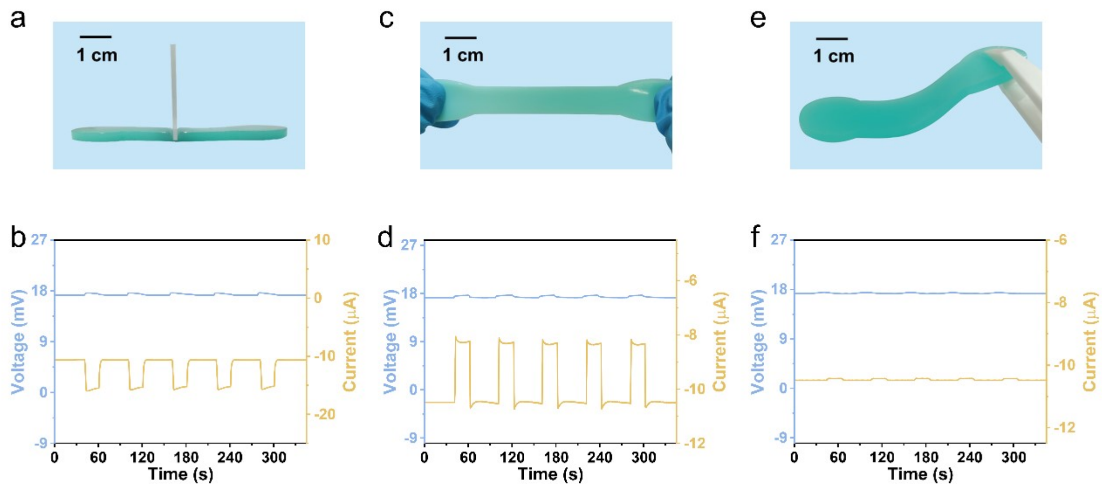

Fig. S21 (a) A photograph of organohydrogel gel being pressed (scale bar: 10 mm). (b) Voltage-time and current-time curves of the organohydrogel gel being repeatedly pressed when Tc= 293 K and Th= 308 K. (c) A photograph of organohydrogel gel being stretched (scale bar: 10 mm). (d) Voltage-time and current-time curves of organohydrogel gel being epeatedly stretched when Tc= 293 K and Th= 308 K. (e) A photograph of organohydrogel gel being bent (scale bar: 10 mm). (f) Voltage-time and current-time curves of the organohydrogel gel being repeatedly bent when Tc= 293 K and Th= 308 K.

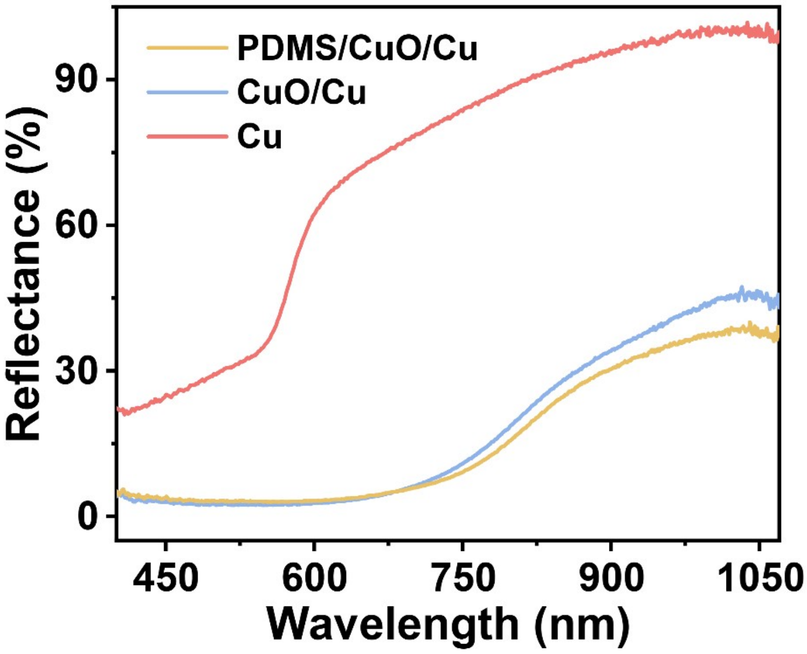

Fig. S22 UV–vis–NIR reflection spectra of PDMS/CuO/Cu foil, CuO/Cu foil, and Cu foil.

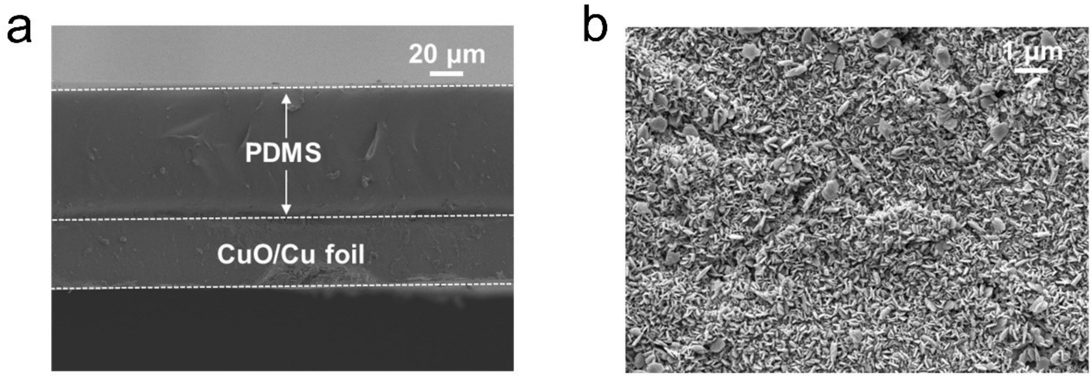

Fig. S23 (a) Cross-sectional SEM image of PDMS/CuO/Cu foil. (b) SEM image of the CuO micro-/nanostructure in CuO/Cu foil.

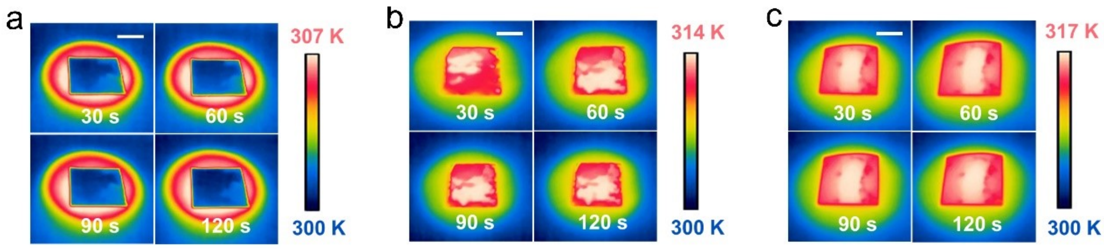

Fig. S24 Corresponding infrared images over time of the PDMS/CuO/Cu foil, CuO/Cu foil, and Cu foil. (Scale bar: 1 cm)

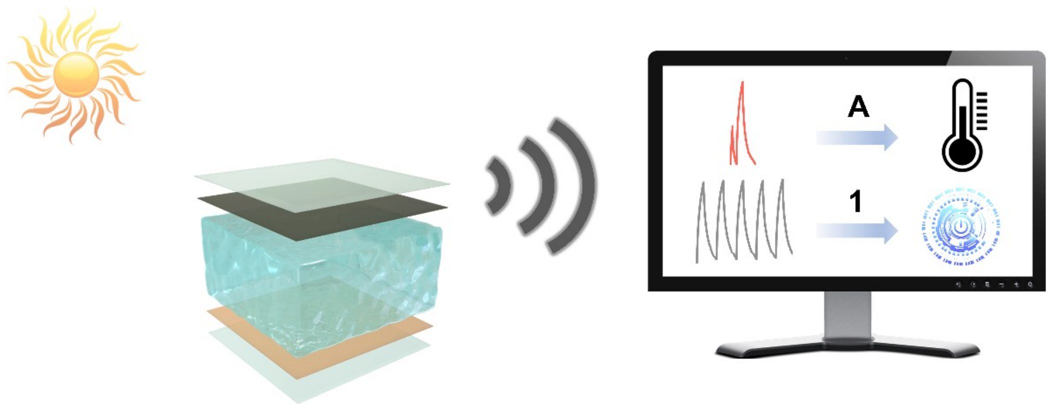

Fig. S25 Panoramic view of the information interaction with the heat sensor of the organohydrogel based on Morse Code.

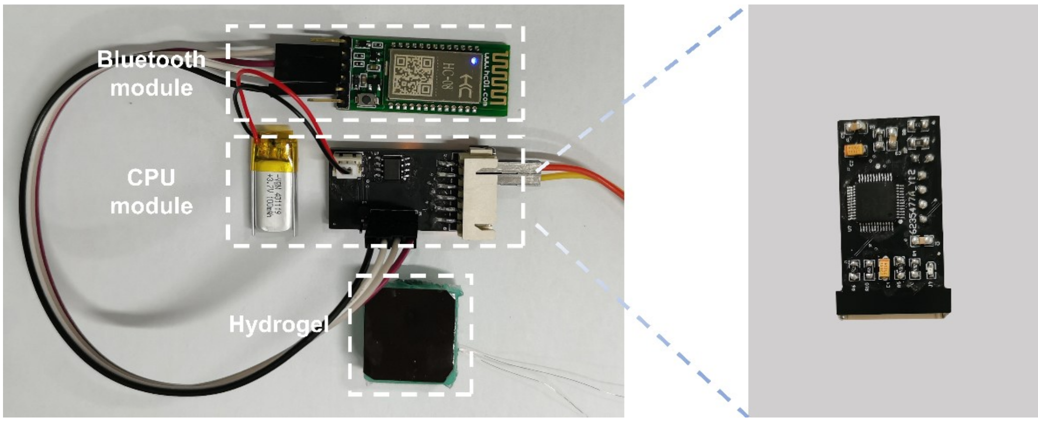

Fig. S26 Wireless Bluetooth transmission device.

Morse codes							
A	• ▬		N	▬ •		0	▬ ▬ ▬ ▬ ▬
B	▬ • • •		O	▬ ▬ ▬		1	• ▬ ▬ ▬ ▬
C	▬ • ▬ •		P	• ▬ ▬ •		2	• ▬ ▬ ▬
D	▬ • •		Q	▬ ▬ • ▬		3	• • • ▬ ▬
E	•		R	• ▬ •		4	• • • • ▬
F	• • ▬ •		S	• • •		5	• • • • •
G	▬ ▬ •		T	▬		6	▬ • • • •
H	• • • •		U	• • ▬		7	▬ ▬ • • •
I	• •		V	• • • ▬		8	▬ ▬ ▬ • •
J	• ▬ ▬ ▬		W	• ▬ ▬		9	▬ ▬ ▬ ▬ •
K	▬ • ▬		X	▬ • • ▬			
L	• ▬ • •		Y	▬ • ▬ ▬			
M	▬ ▬		Z	▬ ▬ • •			

Fig. S27 International Morse Code table.

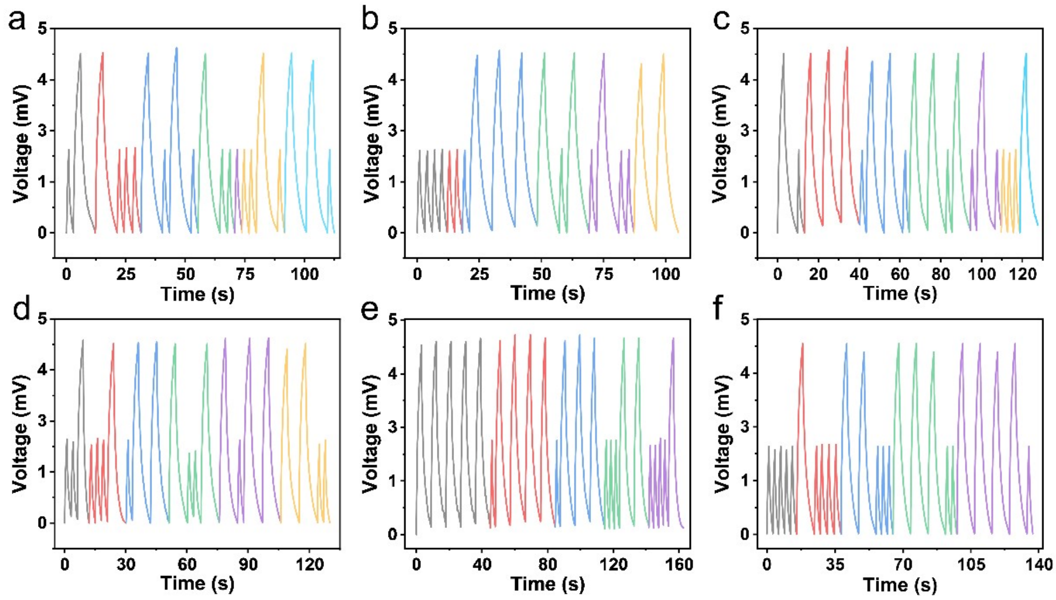

Fig. S28 All letters in the international Morse Code table are indicated. (a) A-G, (b) H-M, (c) N-T, (d) U-Z, (e) 0-4, (f) 5-9.

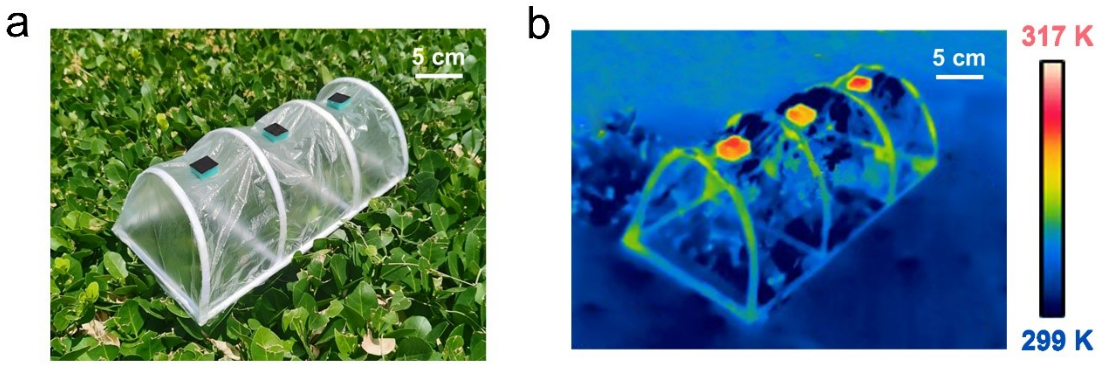

Fig. S29 (a) Photos of the greenhous model. (b) Infrared image of the greenhouse model.

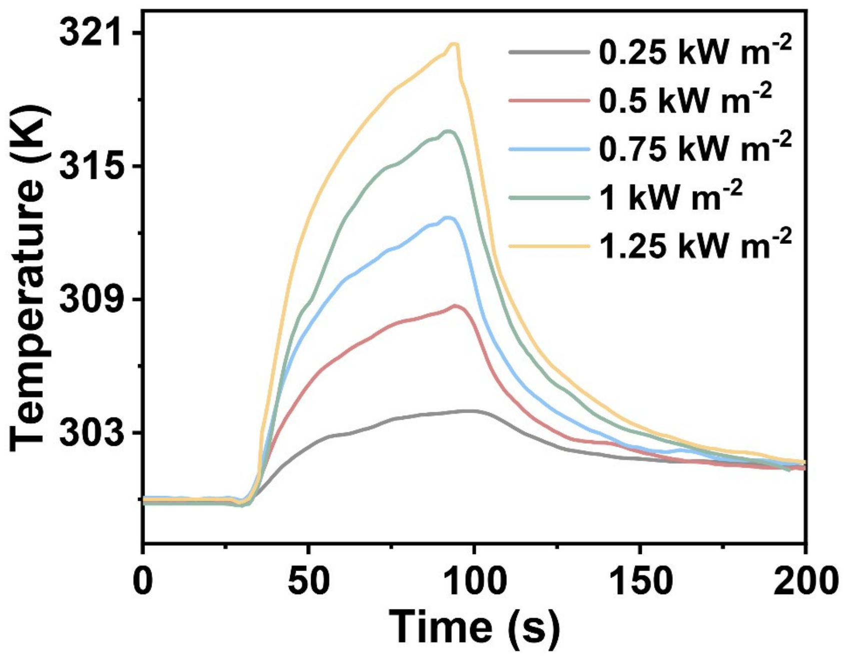

Fig. S30 PDMS/CuO/Cu foil temperature at different optical densities.

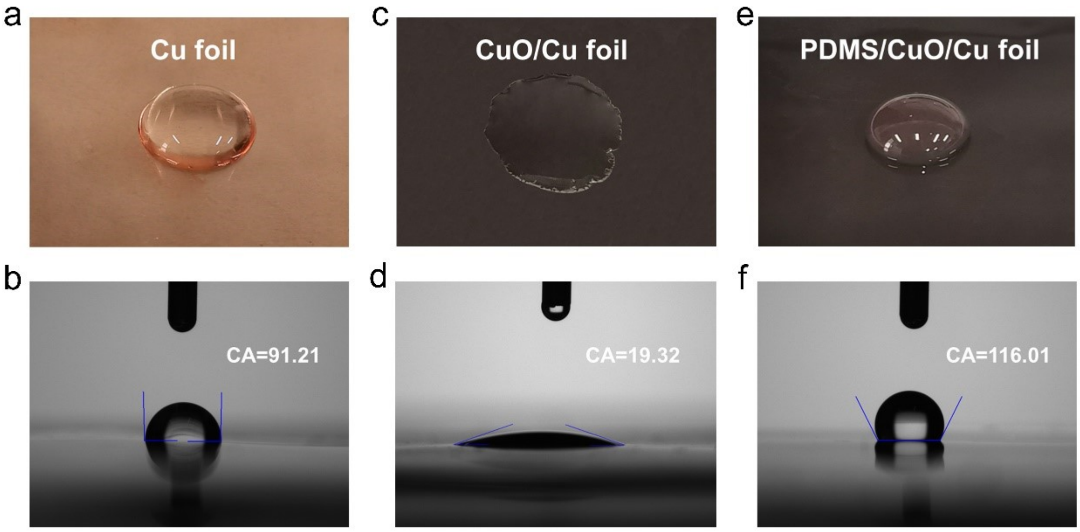

Fig. S31 Photographs of the contact angle tests for hydrophilic and hydrophobic features of Cu foil (a, b), CuO/Cu foil (c, d), and PDMS/CuO/Cu foil (e, f).

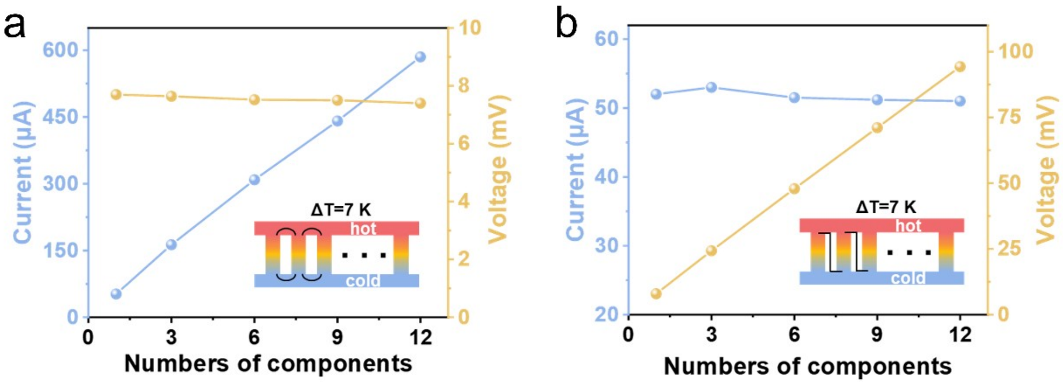

Fig. S32 Output current and output voltage of different number of integrated devices (a) in parallel and (b) in series.

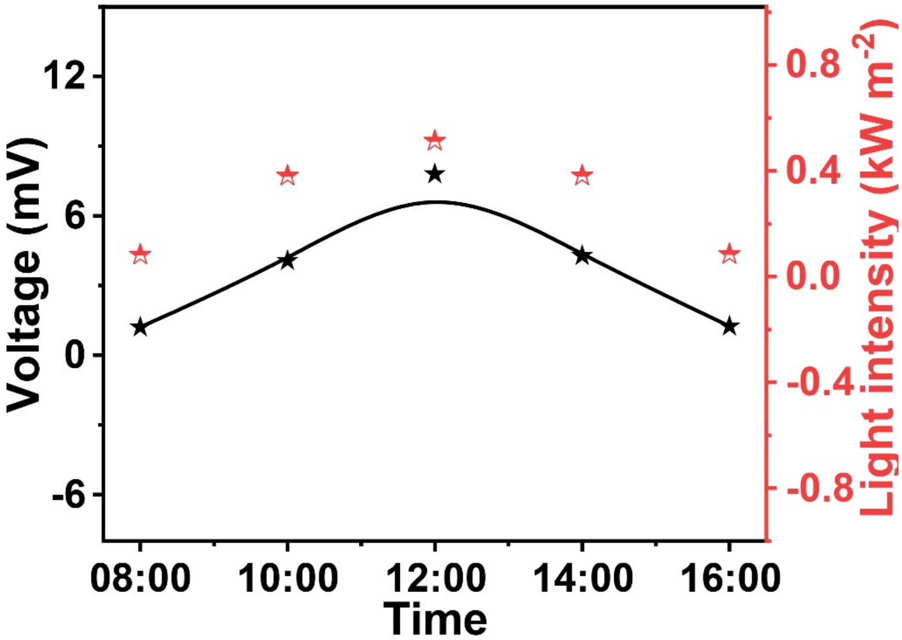

Fig. S33 Output voltage and winter light intensity changing throughout a day.

Stress (kPa)	Stretchability (%)	$\|S_e\|$ (mV K^{-1})	Recyclability	Anti-freezing	Ref.
710	325	1.19	Yes	Yes	This work
97	420	0.63	Yes	Yes	1
260	356	1.43	No	No	2
9	95	1.25	No	No	3
73	225	1.46	Yes	No	4
10.5	500	1.57	No	No	5

Table S1. A comprehensive comparison between the organohydrogel and the previously reported thermogalvanic hydrogels in terms of the comprehensive properties of stress (kPa), stretchability (%), Seebeck coefficient (S_e), recyclability and anti-freezing.

Absorber materials	Electricity type	Solar Intensity (kW m^{-2})	Solar thermal conversion efficiency (%)	Cost ($)	Ref.
PDMS/CuO /Cu	Thermogalvanic (Cu/Cu^{2+})	1	77.3	0.1	This work
Graphite /nonwoven film	Thermoelectric (Bi_2Te_3)	8	72.2	22.1	6
Nitrogen enriched carbon	Piezoelectric (PVDF)	1	90	17	7
CNT modified filter paper	Ionvoltaic(Nafion membrane)	1	75	12	8
r-GO coated fiber	Photovoltaic (Polysilicon)	1	74.6	1.1	9
graphene oxide (rGO)	Piezoelectric (PVDF-TrFE)	1	80	15	10

Table S2. Summary of the absorber materials, electricity type, solar intensity, and cost reported and this work.

Photothermal conversion efficiency calculation.[11] The overall steam generation efficiency (η) can be calculated using the Equation (1).

Equation (1):

$$\eta = (\dot{m}h_{LV})/q_i$$

Where $\dot{m}$ is the solar-driven evaporation rate of water under solar illumination, q_i is the incident power density of solar illumination in process of steam generation experiment, and h_{LV} made up of the sensible heat and the enthalpy of vaporization is calculated using the Equation (2).

Equation (2):

$$h_{LV} = C\Delta T + \Delta h$$

Where C is the specific heat capacity of water and a constant of 4.18 J $g^{-1}K^{-1}$, ΔT is the temperature increase of water, and Δh is the enthalpy of vaporization on the relative temperature.

Supplemental references:

1 X. Li, X. Xiao, C. Bai, M. Mayer, X. Cui, K. Lin, Y. Li, H. Zhang and J. Chen, J. Mater. Chem. C, 2022, **10**, 13789-13796.

2 P. Peng, J. Zhou, L. Liang, X. Huang, H. Lv, Z. Liu and G. Chen, Nano-Micro Lett., 2022, **14**, 81.

3 Y. Zhou, S. Zhang, M. A. Buckingham, L. Aldous, S. Beirne, C. Wu, Y. Liu, G. Wallace and J. Chen, Chem. Eng. J., 2022, **449**, 137775.

4 H. Yang, S. Ahmed Khan, N. Li, R. Fang, Z. Huang and H. Zhang, Chem. Eng. J., 2023, **473**, 145247.

5 J. Shen, Y. Ma, C. Yang, S. Liu, J. Li, Z. Chen, B. Tian and S. Li, J. Mater. Chem. A, 2022, **10**, 7785-7791.

6 X. Li, X. Min, J. Li, N. Xu, P. Zhu, B. Zhu, S. Zhu and J. Zhu, Joule, 2018, **2**, 2477-2484.

7 L. Zhu, M. Gao, C. K. N. Peh, X. Wang and G. W. Ho, Adv. Energy Mater., 2018, **8**, 1702149.

8 P. Yang, K. Liu, Q. Chen, J. Li, J. Duan, G. Xue, Z. Xu, W. Xie and J. Zhou, Energy Environ. Sci., 2017, **10**, 1923-1927.

9 N. Xu, P. Zhu, Y. Sheng, L. Zhou, X. Li, H. Tan, S. Zhu and J. Zhu, Joule, 2020, **4**, 347-358.

10 S. Meng, C. Tang, J. Yang, M. Yang and W. Yang, Adv. Sci., 2022, **9**, 2204187.

11 F. L. Meng, M. Gao, T. Ding, G. Yilmaz, W. L. Ong and G. W. Ho, Adv. Funct. Mater., 2020, **30**, 2002867.